A Surface Composition Study of Niobium after BCP for SRF Cavity in Particle Accelerator

Didi Luo[1], **Changlin Wang**[1,*], **Feng Pan**[2,**]

[1] Institute of Modern Physics, Chinese Academy of Sciences, Nanchang Rd 509, Lanzhou, 730000, China

[2] GLVAC Industrial Technology Research Institute of High Power Devices Co. LTD, Suzhou, 215300, China

E-mail: *wangchanglin@impcas.ac.cn

E-mail: **panfeng@glvac.cn

Abstract. Nitrogen contamination from post-processing significantly affects the performance of niobium superconducting radiofrequency (SRF) cavities. Therefore, several performance-boosting strategies, including nitrogen doping, infusion and chemical acid reactions, have been explored in various studies. Among these studies, some secondary ion mass spectrometry (SIMS) results showed that nitrogen contamination exists on the niobium surface after the buffered chemical polishing (BCP) process. However, the compositions of these nitrogen byproducts were hard to detect. In this work, we calculated the chemical reaction process by the density function theory (DFT), predicted the reaction product, and then analyzed the Nb sample surface after BCP with X-ray Photoelectron Spectroscopy (XPS) to determine the composition of these contaminations.

1. Introduction

The Accelerator Driven Sub-critical System (ADS), which can transmute long-life radioactive waste, is considered as the optimal method of converting spent fuel into short-lived isotopes. As a concept for awaiting verification before widespread implementation, ADS is in the transition from the phase of developing key technologies to the systematic and integrated research.

As one national large-scale scientific instrumentation, the China initiative Accelerator Driven System (CiADS) [1] will be the world's first prototype of ADS facility at the megawatt level to explore the safe and proper nuclear waste disposal technology.

1.1. SRF Cavity

Particle accelerators have extensively adopted superconducting radiofrequency (SRF) cavities to achieve high accelerating gradients and low RF power dissipation [2]. The most frequently used measure of cavity performance is the Q_0 vs. E_{acc} plot (or the "Q vs. E curve"), where E_{acc} is the cavity acceleration gradient, and Q_0 is the intrinsic quality factor given by:

$$Q_0 = \frac{\omega U}{P_{loss}} = \frac{\Gamma}{R_S}, \tag{1}$$

where ω is the operation frequency, U is the storage energy, P_{loss} is the power dissipation, Γ is the cavity geometry factor, and R_S is the surface resistance.

Content from this work may be used under the terms of the Creative Commons Attribution 3.0 licence. Any further distribution of this work must maintain attribution to the author(s) and the title of the work, journal citation and DOI.
Published under licence by IOP Publishing Ltd

Although their power losses are much lower than those of normal conducting RF cavities, superconducting cavities still suffer from multiple degrading effects that limit their performance, such as field emission (FE), multipacting, hydrogen Q-disease, Q-slope (HFQS) and thermal quench, resulting in both a lower Q than ideal theoretical prediction and a drop in Q as E_{acc} increases (i.e. Q-slope). The mechanisms behind some of these degrading effects are still unclear, and a summary can be found in Ref.[3].

1.2. BCP Reaction

Buffered chemical polishing (BCP) acid consists of nitric acid, hydrofluoric acid and phosphoric acid with a volume ratio of 1: 1: X (where X is a number between 1 and 4 that regulates the reaction rate). BCP is a commonly used treatment method for superconducting niobium cavities: it etches away about 100 μm pollution layer to obtain a clean Nb RF surface, thus reducing the RF loss of the superconducting cavity. After the BCP reaction, air exposure generates a native oxide layer ($\sim$ 5 nm, mostly Nb_2O_5) on the niobium surface. Moreover, Tuggle from JLAB has observed nitrogen by secondary ion mass spectrometry (SIMS) on BCP'ed niobium sample [4]. The RF surface is sensitive to surface impurities, which induce additional RF loss. For example, Ref. [5, 6] showed that oxygen vacancies in the oxide layer could be treated as magnetic impurities, and Ref. [7] showed that the Kapitza thermal boundary resistance generates ΔT heating. However, some side or intermediate reaction products, such as niobium nitride or oxynitride, may exist after BCP, and the study of RF dissipation from other byproducts still needs to be completed. Accordingly, studying the generated byproduct is necessary to evaluate the impact of the reaction process on the superconducting cavity's operation.

The overall reaction of BCP acid with niobium is: $Nb + 5\,HF + 5\,HNO_3 \longrightarrow NbF_5 + 5\,NO_2\uparrow + 5\,H_2O$, where the NbF_5 is soluble, and the NO_2 is gas. This work uses the first-principles calculations to explore the chemical reaction process by calculating the interaction between nitric acid and the niobium metal, and then verifies the results by experiments.

2. DFT Calculation

Based on Density functional theory (DFT), we use the siesta [8] program to optimize the architecture and calculate the system's stability. The exchange-correlation potential adopts the generalized gradient approximation (GGA) in the form of Perdew Burke Ernzerhof (PBE) [8]. In the calculation, we constructed a three-layer stack of niobium atoms and simulated the niobium surface by fixing the underlying atoms. In the Periodic boundary conditions, we use a unit cell with the size of 15 Å $\times$ 15 Å $\times$ 35 Å to simulate discrete HNO_3 molecules and the vacuum layer on the metal surface. Brillouin zone in inverted space adopted Monkhorst Pack grid centered on Γ point for sampling, using a k point grid of $2 \times 2 \times 1$. All lattice structures in this work were optimized using the conjugate gradient (CG) method [9], with a force convergence standard of 10^{-2} eV/Å.

2.1. Adsorption of Single HNO_3 Molecules on Nb Surface

The Nb (110) surface is the most stable, so we first optimized the structure of the Nb metal block and cut a thin layer structure containing three layers of atoms along the (110) surface to simulate the (110) surface of the Nb bulk. We also constructed a single HNO_3 molecular structure and optimized it. The optimized Nb (110) surface and HNO_3 molecular structure are shown in Fig.1. All HNO_3 atoms are in the same plane. To simulate the reaction process of HNO_3 molecules on the Nb (110) surface, we set up three initial configurations, allowing HNO_3 molecules to adsorb at varied positions on the Nb surface with distinct postures.

The first configuration is shown in Fig.2, where the HNO_3 molecule lies flat on the Nb surface and the N atom is next to a Nb atom. After this initial structural optimization, the HNO_3 molecule decomposes and forms O, OH, and NO atoms or groups that are adsorbed

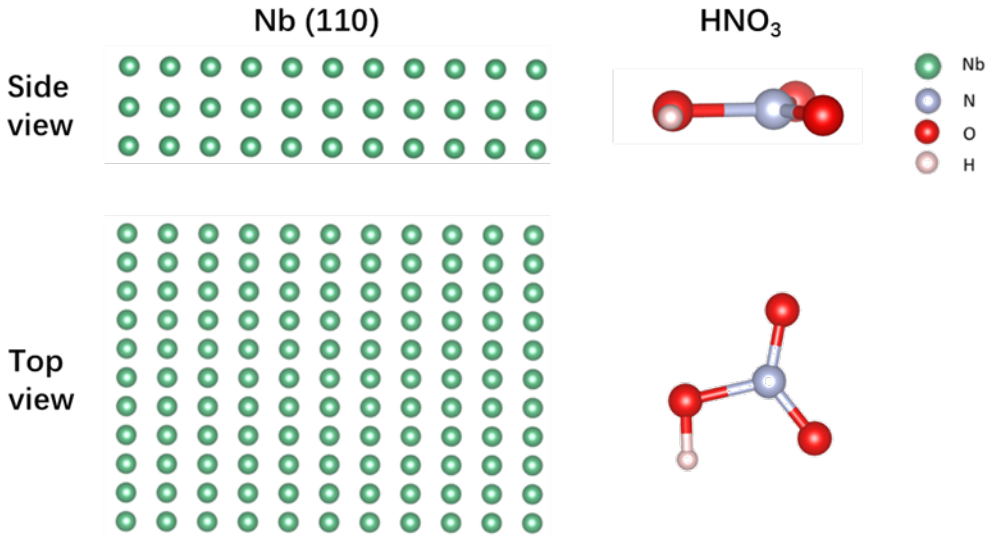

Figure 1. Schematic diagram of the structure of Nb (110) surface (left) and isolated HNO_3 molecule (right)

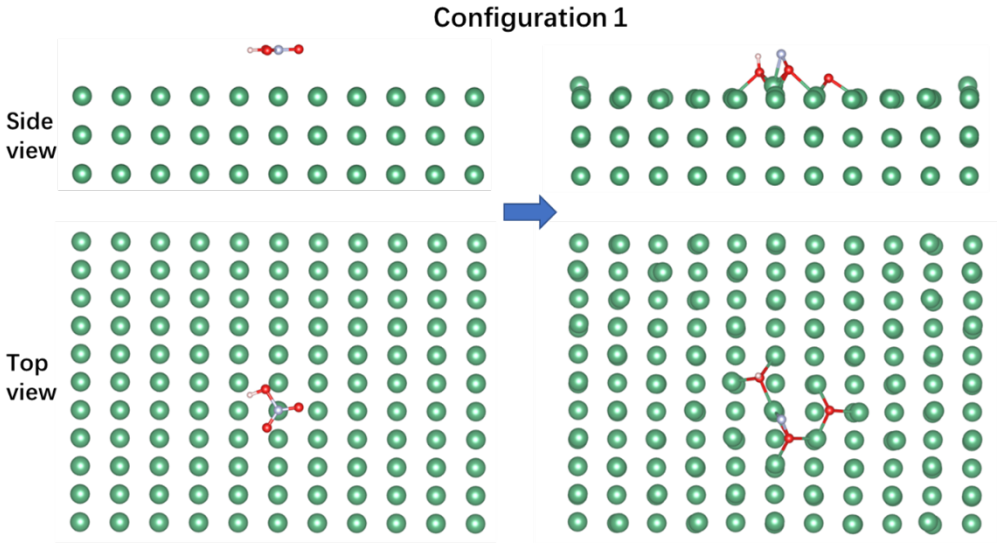

Figure 2. Schematic diagram of the structure of a single HNO_3 molecule adsorbed on Nb surface configuration 1 before and after optimization.

on the Nb surface, respectively, and are all adsorbed on the metal surface in the form of O atoms bonding with three neighboring Nb atoms. The calculated adsorption energy of HNO_3 molecule corresponding to the optimized structure is 6.822 eV (defined as the energy of the pure Nb (110) surface plus the energy of isolated HNO_3 molecules, minus the total energy of the optimized structure after HNO_3 adsorption on the Nb surface), which is the highest of the three configurations. This reaction generates oxides and oxynitrides.

The second configuration is shown in Fig.3, where the HNO_3 molecule remains flat on the Nb surface. Unlike configuration 1, two O atoms are next to the surface Nb atoms. After structural optimization, HNO_3 molecules still decompose, forming OH and NO_2 groups adsorbed on the

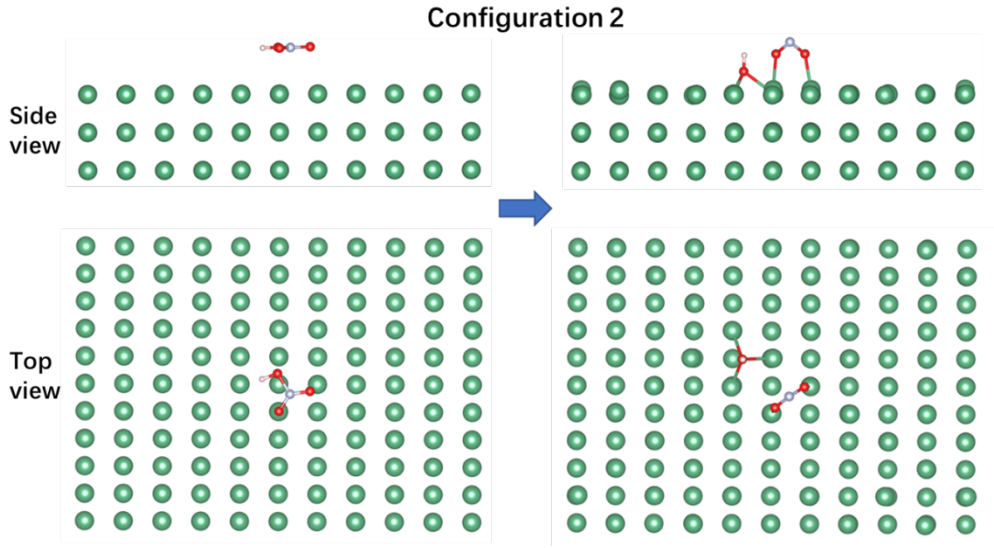

Figure 3. Schematic diagram of the structure of a single HNO_3 molecule adsorbed on Nb surface configuration 2 before and after optimization.

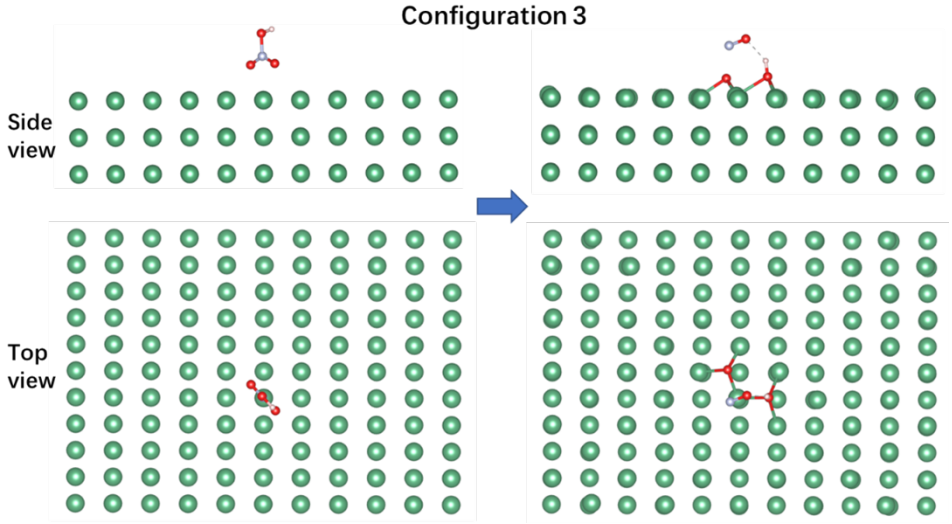

Figure 4. Schematic diagram of the structure of a single HNO_3 molecule adsorbed on Nb surface configuration 3 before and after optimization.

surface of Nb, respectively. OH is connected to three adjacent Nb atoms through O atoms, while NO_2 is adsorbed onto the metal surface through two O atoms connected to one Nb atom, respectively. This structure's adsorption energy is 4.985 eV, which is the lowest of the three configurations. This reaction generates oxynitrides.

The third configuration is shown in Fig.4, where the HNO_3 molecule is initially perpendicular to the Nb surface with two O atoms next to the metal surface. After optimization, one NO molecule detached from the metal surface, and O and OH were adsorbed on the surface of Nb, also through the bonding between O atoms and Nb atoms. For this case, the adsorption energy is 5.499 eV, between configurations 1 and 2. This reaction generates oxides.

From these results, we find that HNO_3 molecule always decomposes into small groups to

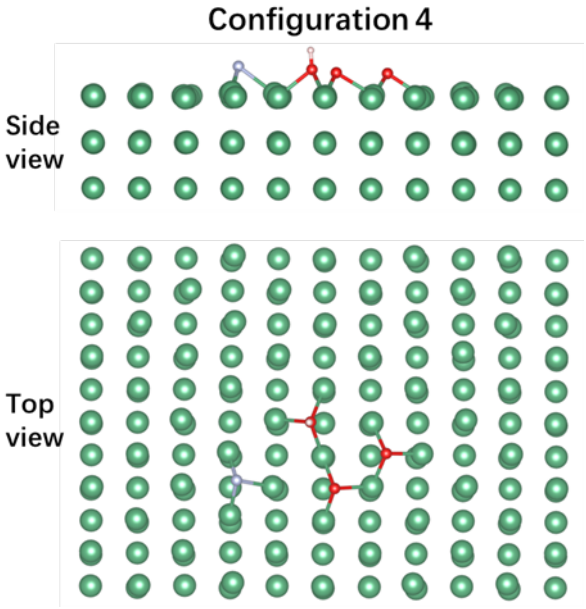

Figure 5. Schematic diagram of the structure of a single HNO_3 molecule adsorbed on Nb surface configuration 4 after optimization.

adsorb on the Nb (110) surface. The atoms and groups obtained from the decomposition of the most stable configuration 1 (i.e. the structure with the highest adsorption energy) are adsorbed on the Nb surface in a more dispersed form. The HNO_3 molecule is more inclined to bond with surface metal atoms to obtain a more stable structure.

We then constructed a configuration 4 structure to disperse and adsorb the N and O atoms in the HNO_3 molecule onto the Nb surface as much as possible. As shown in Fig.5, after optimization, the N atom and three O atoms all bond with three neighbouring Nb atoms, forming dispersed N, O, and OH. The calculated adsorption energy is 11.401 eV, significantly higher than the first three configurations. This high adsorption energy indicates that configuration 4 is the most stable case if the situation exists; however, this stable state may need to cross an energy barrier. This reaction generates oxides and nitrides.

2.2. Adsorption of Double HNO_3 Molecules on Nb Surface

To simulate the reaction of concentrated nitric acid on the Nb surface, we further calculated the adsorption of two HNO_3 molecules on the Nb surface considering the interaction between HNO_3 molecules. As shown in Fig.6, we placed two HNO_3 molecules connected by hydrogen bonds between H and O that lie flat on the surface of Nb. After optimization, HNO_3 molecules were decomposed into NO_2, NO, H_2O and O that adsorbed on the metal surface. The adsorption energy is 9.867 eV. The results also show that H and OH between adjacent HNO_3 molecules easily form water molecules, and this reaction still generates oxides and oxynitrides.

After optimization, the NO_2, NO, and O all bond with multiple Nb atoms, while H_2O only bonds with one Nb atom through the O atom, resulting in the easy departure of the H_2O molecule. Thus, we constructed two configurations after removing water molecules, as shown in Fig.7. Configuration 2 is optimized by removing H_2O from configuration 1, while configuration 3 disperses N and O atoms as much as possible on the Nb surface, yielding corresponding adsorption energies of 11.653 eV and 22.015 eV, respectively. These values show that the energy of N and O atoms adsorbing on the Nb surface is much lower than NO or NO_2 groups. For

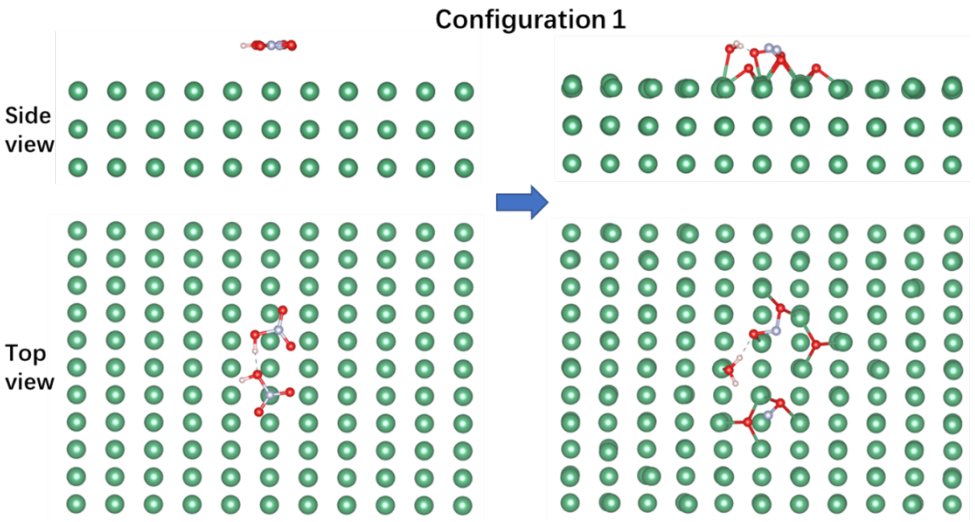

Figure 6. Schematic diagram of the structure of two HNO_3 molecules adsorbed on Nb surface configuration 1 before and after optimization.

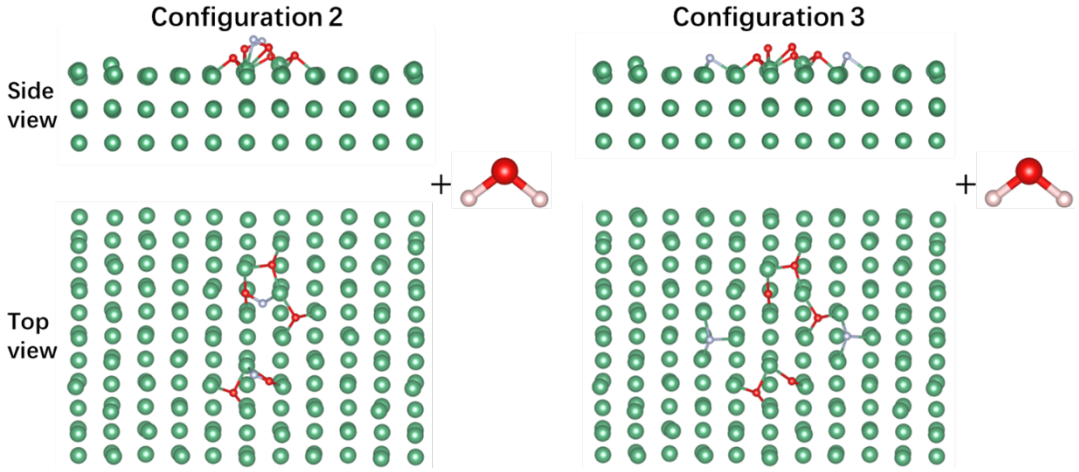

Figure 7. Schematic diagram of the structure of two HNO_3 molecules adsorbed on Nb surface configuration 2 and 3 after optimization.

configuration 3, the surface may generate oxides and nitrides when above specific temperatures.

Subsequently, we investigated the potential barriers for forming oxides and nitrides from nitrogen oxide groups. As shown in Fig.8, we take configuration 1 directly optimized by two HNO_3 molecules as the initial structure, and move the N atoms not bonded to the metal surface to the nearby Nb atoms to form the dispersed adsorbing atoms as the target structure (i.e. configuration 4) and calculate the transition state structure from configuration 1 to configuration 4 and the corresponding energy barrier.

The primary transformation from configuration 1 to configuration 4 is that both N atoms break the bond with the O atoms and connect to the Nb atoms. The transition state structure is similar to configuration 1. During the exploration of the transition state, we found that when the structure transforms from configuration 1 to configuration 4, a slight structural change will lead to the system's total energy decrease, only needing to cross a shallow barrier ($\Delta E = 53$

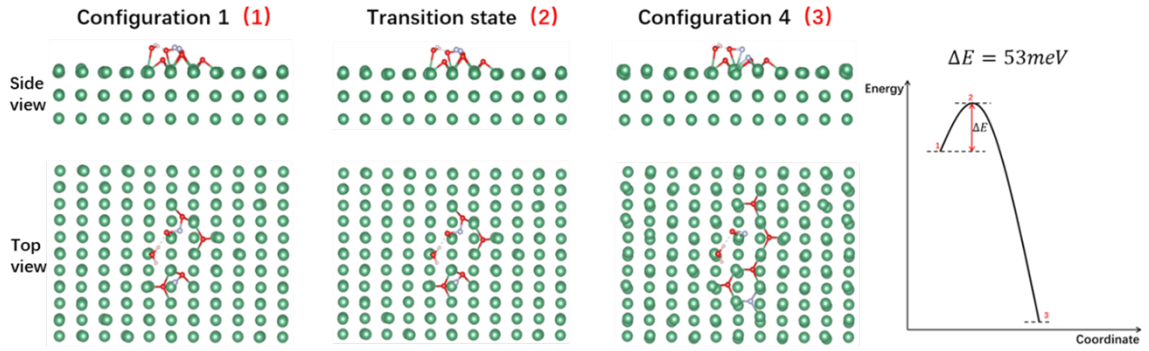

Figure 8. Schematic diagram of the structural change and energy barrier required for the adsorption of double HNO_3 molecules on the Nb surface from configuration 1 through a transition state to configuration 4. The structures represented by the red numbers 1, 2 and 3 in the energy barrier graph (right 1) correspond to the left configuration 1, transition state and configuration 4 structures, respectively.

meV). The transitions from configuration 1 result to configuration 4 decrease the total energy by 7.625 eV, indicating significantly higher stability. Once the system crosses the barrier, the surface nitrides will be very stable.

3. Experiments

We ordered the RRR = 300 Nb sheets from NIN [10]; both sheets were cold rolled to 1 mm and annealed at 700 °C for 10 hours. We performed BCP on the samples for about 100 μm, and then did XPS analysis to study the niobium surface components.

3.1. Bulk Nb Reacts with BCP 100 μm: Same as Cavity Process

To characterize the composition in detail, we performed X-ray Photoelectron Spectroscopy (XPS) on the Nb sample. The equipment is Thermo Scientific K-Alpha+ from ThermoFisher, the vacuum in the chamber is about 5×10^{-9} mbar, the X-Ray source is Mono AlKa (1486.6 eV, 12 KV, 6 mA), the scan mode is CAE, and the work function is 4.2 eV.

Fig.9 shows the XPS survey of bulk niobium reaction with BCP for 100 μm (a). This result shows only O, C and Nb signals. Here, carbon absorption is normal contamination for XPS results. Tuggle has observed nitrogen by SIMS on BCP'ed niobium sample [4]: nitrogen element mostly stays on the surface 0.05 μm and only has a very trace amount, making the detection very difficult. For this BCP sample, we have one hypothesis that the niobium surface roughness after 100 μm BCP reaction is μm-level ($R_p \sim 5\mu m$), resulting in difficult XPS signal detection for the tiny amount of nitrogen. Hence, we need to rule out the high roughness influence. One possible way is to coat niobium on a very smooth substrate that does not react with BCP at the reaction temperature (room temperature). Niobium films growing on Al_2O_3 substrate were selected as the target.

3.2. BCP Light Reaction (0.3 μm) with 2 μm Nb Coating on Al_2O_3 Sample

In order to reduce the roughness impact, we performed niobium magnetron sputtering on an alumina substrate to obtain $\sim$ 2 μm niobium film. We then put the sample into BCP acid for a short period (20 seconds) and washed it with ultra-pure water. The reaction etched away about 0.3 μm Nb, and roughness should be less than 1 μm after the reaction. We later performed XPS to characterize the surface component and Nb oxidation state, as shown in Fig.9 (b). We also

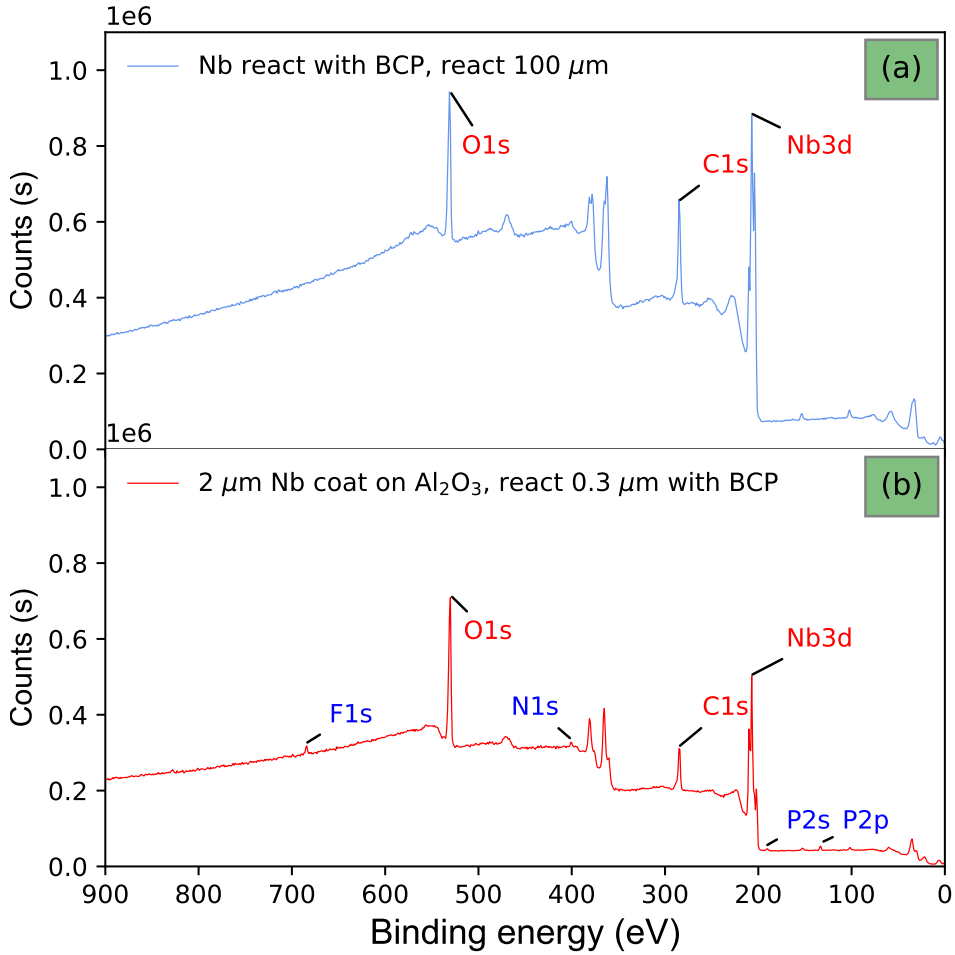

Figure 9. XPS survey of the bulk niobium react with BCP for 100 μm (a), and the 2 μm niobium coating on Al_2O_3 and react with BCP for 0.3 μm (b). The characteristic peaks are marked in the corresponding positions.

performed Ar^+ sputtering to obtain the sample composition profiling, as shown in Fig.10. We found the listed information:

(i) Unlike the baseline BCP 100 μm result, some weak F, N, and P peaks emerge from the Nb film sample XPS (Fig.9), indicating this strategy improved the test sensitivity for low concentration elements.

(ii) Fig.10 shows that N and P disappeared after only 7 seconds Ar^+ sputtering, indicating the N and P elements exist only in the first 0.6 nm, agreed with the results in Ref.[4].

(iii) The F1s signal stays for all the sputtering results. Even if HF does not react with Al_2O_3 below 1000 °C, it may still easily be absorbed by the Al_2O_3 surface and influence the sample XPS result.

(iv) The O1s signals stay the same during the 35 seconds of sputtering, indicating the Nb film is highly oxidized in the first 3 nm. This oxidization could be from the BCP reaction or from the Nb film coating process.

Thus, we conclude that the Nb film reacting with the BCP strategy has too many uncertainties, so we chose another way to eliminate the high-roughness parameter of the BCP sample.

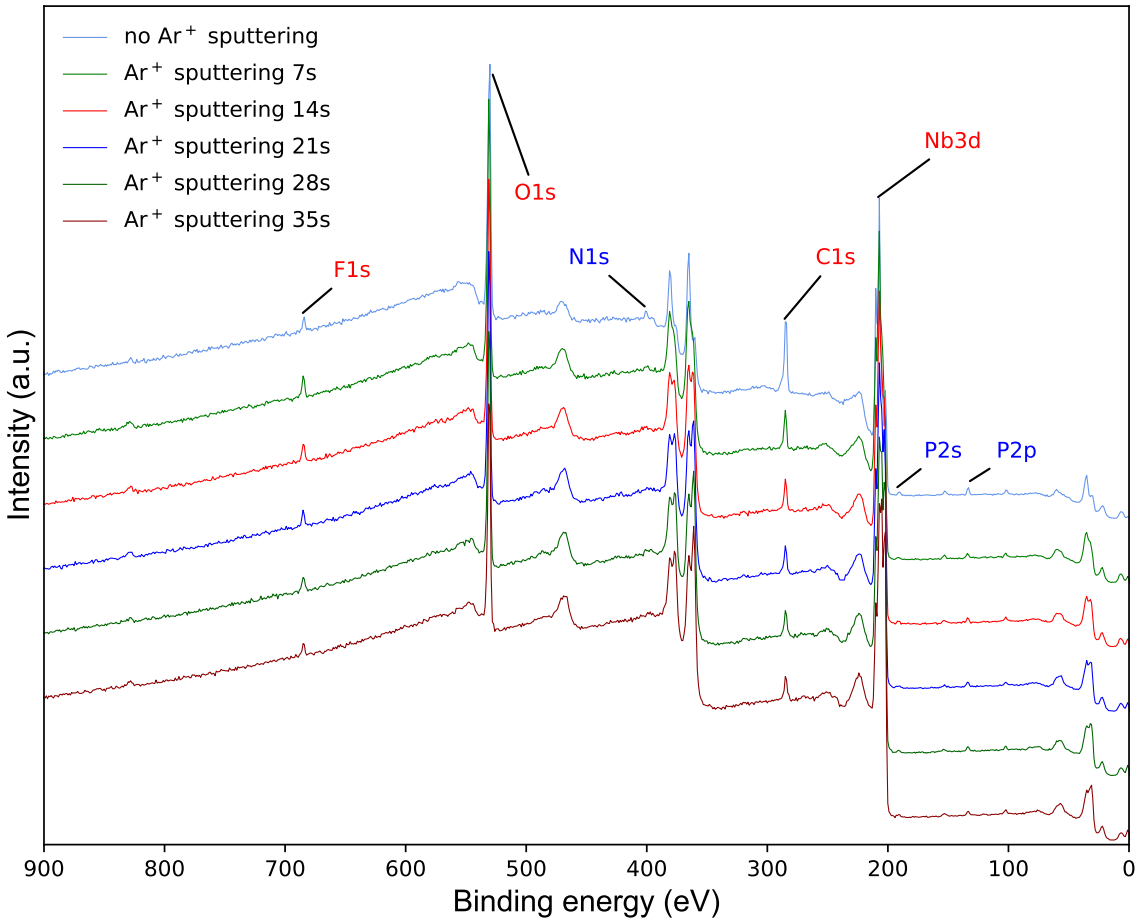

Figure 10. The XPS signal of Ar^+ sputtering process for the 2 μm niobium coating on Al_2O_3 and react with BCP for 0.3 μm sample. The Ar^+ sputtering rate is about 4.8 nm/min [11].

3.3. BCP Light Reaction (1 μm) with Mechanical Polished Nb Sample

We performed mechanical polishing for a bulk niobium sample, obtained a nanometer-level polished surface, and let the sample react with BCP acid for one minute (etched about 1 μm), rinsed with ultra-pure water. In this case, the roughness should still be less than 1 μm. We then characterized the surface by XPS (Fig.11 (c)). We also performed Ar^+ sputtering to obtain the sample composition change with depth, as in Fig.11 (d). From the test, we found:

(i) Some F, N, and P signals exist on the 1-μm-reaction sample; the N and P peaks are even higher than the Nb film sample, indicating this strategy improved the test sensitivity for low-concentration elements.

(ii) The O1s signals reduced during the 34 seconds of sputtering, indicating that the Nb oxides are mostly located in the first 3 nm. Unlike the film-coating on Al_2O_3 sample, the mechanical polishing does not oxidize the high-purity bulk niobium sample in the deep.

3.4. Preliminary Results of the N form on Nb surface

We thus acquired the high-resolution signals of the N1s (Fig.12), O1s (Fig.13) and Nb3d (Fig.14) to study the oxidation state of niobium. For N1s, the N-O dominates the signal, indicating that configuration 1 in Fig.6 or configuration 2 in Fig.3 results happen, which means the NO or NO_2

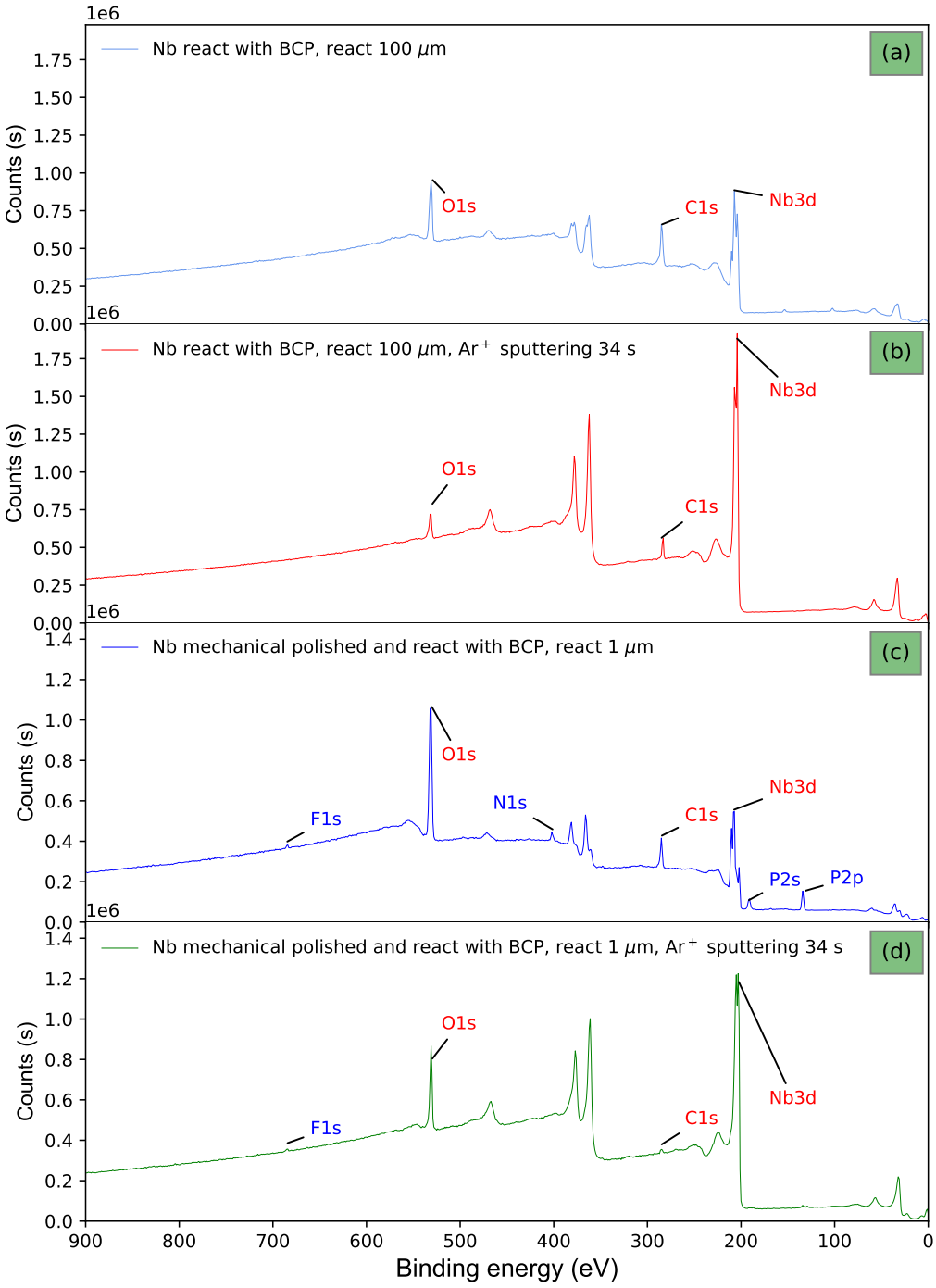

Figure 11. XPS survey of the bulk niobium react with BCP for 100 μm (a & b), and the mechanically polished bulk niobium react with BCP for 1 μm (c & d). Please notice the y-axis are different for the two samples. The Ar^+ sputtering rate is about 4.8 nm/min [11]).

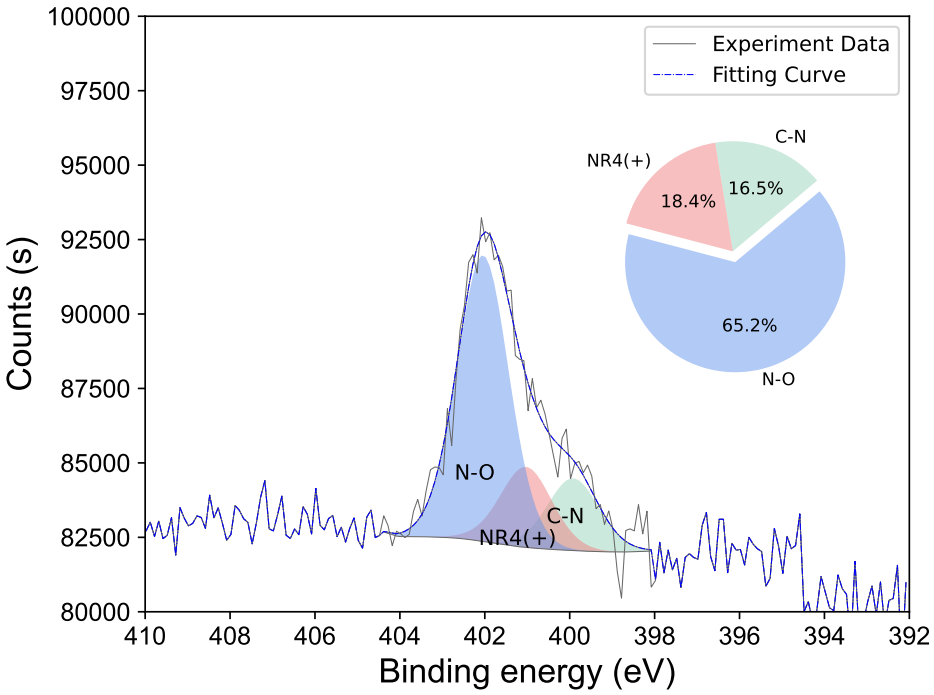

Figure 12. High-resolution XPS scans of N1s region for the niobium sample.

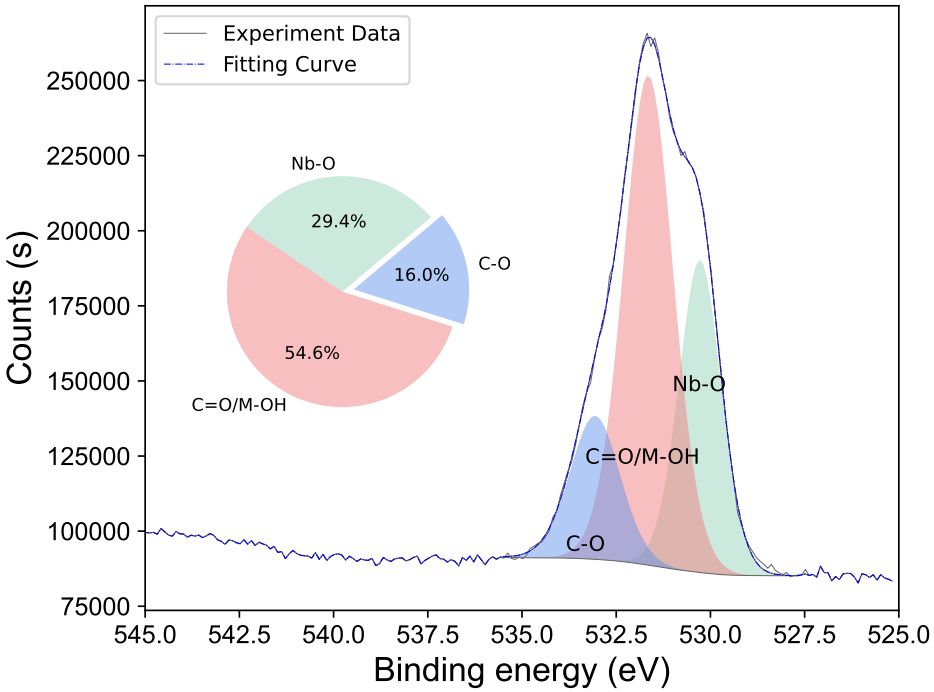

Figure 13. High-resolution XPS scans of O1s region for the niobium sample. The valence state of Nb-O is Nb^{2+}.

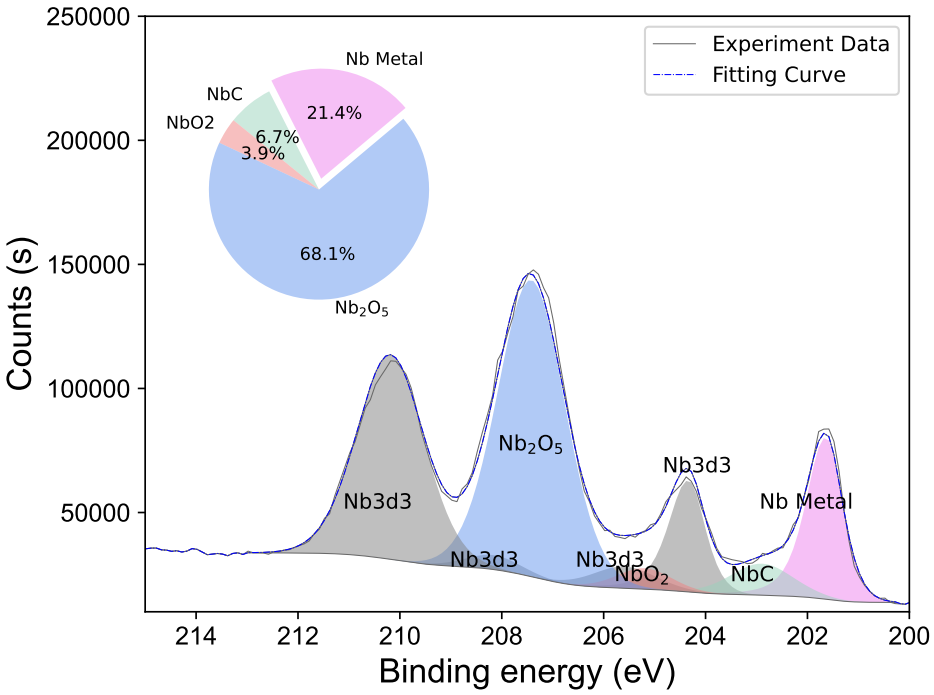

Figure 14. High-resolution XPS scans of Nb3d region for the niobium sample. The Nb3d3 signals are filled grey. The valence state of Nb is Nb^{2+} in NbC, Nb^{4+} in NbO_2 and Nb^{5+} in Nb_2O_5, respectively.

group absorbed on the niobium surface. Fig.14 also shows the absence of Nb-N bonding. The XPS of N1s and Nb3d high-resolution signal has no niobium nitride composition, indicating that configuration 4 in Fig.5 does not exist. The barrier $\Delta E = 53$ meV calculated from Fig.7 and Fig.8 is not crossed. Fig.13 shows Nb-O bonding and carbon contamination, maybe due to the low concentration of the NO group.

4. Conclusion

In summary, we used the first-principles calculation to simulate the interaction between a single and two HNO_3 molecules in contact with the surface of Nb metal (110). Calculations indicated that HNO_3 molecules are easily decomposed into OH, NO, and NO_2 groups adsorbed on the surface when in contact with Nb. The reaction can generate oxides and oxynitrides (configuration 1, 2 & 3 for single HNO_3 absorption, configuration 1 & 2 for double HNO_3 absorption) or oxides and nitrides (configuration 4 for single HNO_3 absorption, configuration 3 & 4 for double HNO_3 absorption). Further calculation showed that nitride formation needs to cross a $\Delta E = 53$ meV barrier.

We then did experiments to explore the byproducts of the BCP reaction. We first let the Nb bulk sample react with BCP for 100 μm, the same as the cavity treatment, and did not find the N signal in the XPS. After improving the niobium surface roughness by coating niobium on an alumina substrate and mechanically polishing with a light BCP reaction, we successfully obtained N, F, and P peaks on the niobium surface. High-resolution XPS scans of N1s, O1s and Nb3d only showed the existence of N-O bonding, indicating the BCP reaction at room temperature did not cross the 53 meV barrier.

In the future, we will further optimize the surface condition to get higher N signals, explore

the F and P interactions with the niobium surface, and get a complete picture of BCP reaction byproducts. This strategy can also be applied to characterize the chemical reactions of the prevalent nitrogen doping and infusion techniques.

Acknowledgments
The work was supported by the Young Scientists Fund of the National Natural Science Foundation of China (Grant NO. 12105335).

References

[1] Ciads, Website, https://english.imp.cas.cn/research/facilities/CIADS/ (2022).
[2] M. Tigner, Rf superconductivity for accelerators–is it a hollow promise?, IEEE Transactions on Magnetics 15 (1979) 15–20.
[3] H. Padamsee, History of gradient advances in srf (2020). arXiv:2004.06720.
[4] J. Tuggle, A. Palczewski, C. Reece, F. Stevie, M. Kelley, Investigation of low-level nitrogen in niobium by secondary ion mass spectrometry, in: Proceedings of LINAC2016, Virginia Polytechnic Institute and State University, East Lansing, MI, USA, 2016.
[5] T. Proslier, J. Zasadzinski, L. Cooley, C. Antoine, J. Moore, J. Norem, M. Pellin, K. Gray, Tunneling study of cavity grade nb: Possible magnetic scattering at the surface, Applied Physics Letters 92 (04 2009). doi:10.1063/1.2913764.
[6] M. Wenskat, J. Čižek, M. O. Liedke, M. Butterling, M. Stiehl, G. D. L. Semione, C. Backes, C. Bate, O. Melikhova, E. Hirschmann, A. Wagner, H. Weise, A. Stierle, M. Aeschlimann, W. Hillert, Vacancy dynamics in niobium and its native oxides and their potential implications for quantum computing and superconducting accelerators, Phys. Rev. B 106 (2022) 094516. doi:10.1103/PhysRevB.106.094516.
URL https://link.aps.org/doi/10.1103/PhysRevB.106.094516
[7] J. D. Halbritter, Degradation of superconducting rf cavity performances by extrinsic properties, 11th Workshop on RF-Superconductivity (SRF 2003), Lübeck, September 8-12, 2003 Proc.on CD-ROM MoP44 Hamburg : DESY, 2004, 42.02.02; LK 01 (2005).
[8] J. M. Soler, E. Artacho, J. D. Gale, A. García, J. Junquera, P. Ordejón, D. Sánchez-Portal, The siesta method for ab initio order-n materials simulation, Journal of Physics: Condensed Matter 14 (11) (2002) 2745. doi:10.1088/0953-8984/14/11/302.
URL https://dx.doi.org/10.1088/0953-8984/14/11/302
[9] M. R. Hestenes, E. Stiefel, Methods of conjugate gradients for solving linear systems, Journal of research of the National Bureau of Standards 49 (1952) 409–435.
[10] Nin, Website, http://www.c-nin.com/ (2022).
[11] M. Yu, G. Pu, Y. Xue, S. Wang, S. Chen, Y. Wang, L. Yang, Z. Wang, T. Zhu, T. Tan, Y. He, S. Huang, K. Zhang, The oxidation behaviors of high-purity niobium for superconducting radio-frequency cavity application in vacuum heat treatment, Vacuum 203 (2022) 111258. doi:https://doi.org/10.1016/j.vacuum.2022.111258.
URL https://www.sciencedirect.com/science/article/pii/S0042207X22003827